RADC-TR-76-52
Final Technical Report
March 1976

AEROSOL ATTENUATION IN THE 2 - 4 μm REGION

Aerodyne Research, Inc.

Sponsored by
Defense Advanced Research Projects Agency
ARPA Order 1279

Approved for public release;
distribution unlimited.

The views and conclusions contained in this document are those of the authors and should not be interpreted as necessarily representing the official policies, either expressed or implied, of the Defense Advanced Research Projects Agency or the U. S. Government.

Rome Air Development Center
Air Force Systems Command
Griffiss Air Force Base, New York 13441

This report has been reviewed by the RADC Information Office (OI) and is releasable to the National Technical Information Service (NTIS). At NTIS it will be releasable to the general public including foreign nations.

This report has been reviewed and is approved for publication.

APPROVED: James W Cusack

JAMES W. CUSACK
Project Engineer

Do not return this copy. Retain or destroy.

AEROSOL ATTENUATION IN THE 2 - 4 μm REGION

Dr. Robert C. Sepucha
Dr. David M. Mann

Contractor: Aerodyne Research, Inc.
Contract Number: F30602-74-C-0282
Effective Date of Contract: 20 May 1974
Contract Expiration Date: 15 November 1975
Amount of Contract: $174,250.00
Program Code Number: 5E20
Period of work covered: May 74 - Nov 75

Principal Investigators: Dr. Robert C. Sepucha
Phone: 617 272-1100
Dr. David M. Mann
Phone: 617-272-1100

Project Engineer: James W. Cusack
Phone: 315 330-3145

This research was supported by the Defense Advanced Research Projects Agency of the Department of Defense and was monitored by James W. Cusack (OCSE), Griffiss AFB NY 13441.

UNCLASSIFIED
SECURITY CLASSIFICATION OF THIS PAGE (When Data Entered)

REPORT DOCUMENTATION PAGE

READ INSTRUCTIONS BEFORE COMPLETING FORM

1. REPORT NUMBER: RADC-TR-76-52	2. GOVT ACCESSION NO.
3. RECIPIENT'S CATALOG NUMBER	
4. TITLE (and Subtitle): AEROSOL ATTENUATION IN THE 2-4 Micrometers REGION	5. TYPE OF REPORT & PERIOD COVERED: Final Technical Report 20 May 74 — 20 Nov 75
6. PERFORMING ORG. REPORT NUMBER: ARI-RR-77	
7. AUTHOR(s): Robert C. Sepucha, David M. Mann	8. CONTRACT OR GRANT NUMBER(s): F30602-74-C-0282, ARPA Order-1279
9. PERFORMING ORGANIZATION NAME AND ADDRESS: Aerodyne Research, Inc. 20 South Avenue Burlington MA 01803	10. PROGRAM ELEMENT, PROJECT, TASK AREA & WORK UNIT NUMBERS: 62301E, 1279[illegible], AF — 127905
11. CONTROLLING OFFICE NAME AND ADDRESS: Defense Advanced Research Projects Agency 1400 Wilson Blvd Arlington VA 22209	12. REPORT DATE: Mar[illegible]76
	13. NUMBER OF PAGES: 30 (123 p.)
14. MONITORING AGENCY NAME & ADDRESS (if different from Controlling Office): Rome Air Development Center (OCSE) Griffiss AFB NY 13441	15. SECURITY CLASS. (of this report): UNCLASSIFIED
	15a. DECLASSIFICATION/DOWNGRADING SCHEDULE: N/A

16. DISTRIBUTION STATEMENT (of this Report)

Approved for public release; distribution unlimited.

17. DISTRIBUTION STATEMENT (of the abstract entered in Block 20, if different from Report)

Same

18. SUPPLEMENTARY NOTES

RADC Project Engineer:
James W. Cusack (OCSE)

Copies are available in DDC.

19. KEY WORDS (Continue on reverse side if necessary and identify by block number)

Aerosol
DF Laser
Aerodol Infrared Absorption
Aerosol Infrared Extinction
White Cell

20. ABSTRACT (Continue on reverse side if necessary and identify by block number)

This report describes an experimental facility constructed to measure the extinction and scattering of DF laser radiation by atmospheric aerosols. The details of the apparatus, the theory of the measurements, and calibration results are presented.

DD FORM 1 JAN 73 1473 EDITION OF 1 NOV 65 IS OBSOLETE

UNCLASSIFIED
SECURITY CLASSIFICATION OF THIS PAGE (When Data Entered)

390 112

TABLE OF CONTENTS

Section		Page
1	INTRODUCTION AND SUMMARY	1
2	EXPERIMENTAL INVESTIGATION	3
	2.1 Introduction	3
	2.2 Extinction Measurement	3
	2.2.1 Theory of the Measurement	3
	2.2.2 Description of the Optical Train and the White Cell	8
	2.2.3 Detection System	10
	2.2.4 Aerosol Handling System	12
	2.2.5 Calibration Procedure	14
	2.3 Scattering Measurement	16
	2.3.1 Theory of the Measurement	16
	2.3.2 Description of the Apparatus	18
	2.3.3 Calibration Procedure	19
	2.4 Aerosol Characterization	23
	2.5 Results	26
	REFERENCES	30

LIST OF ILLUSTRATIONS

Figure		Page
2.1	Schematic of Experimental Apparatus	4
2.2	Laboratory Layout of Experimental Measurements: Scattering Cell and Control Panel	5
2.3	Laboratory Layout of Experimental Measurements: Optics Tables, Laser, and White Cell	6
2.4	Schematic of Electronics for Extinction Measurement	11
2.5	External View of 400m White Cell	12
2.6	Primary Aerosol and Gas Handling Systems	13
2.7	Calibration for Extinction Measurements at 3.8 μm	15
2.8	Schematic of Aerosol Scattering Cell	16
2.9	N_2O Absorption Coefficient and Operating Levels for Scattering Calibration	21

1. INTRODUCTION AND SUMMARY

The experimental program described in this final report was designed to obtain data on the fundamental optical properties of atmospheric aerosols at DF laser wavelengths in the 2 to 4 μm spectral region.

Atmospheric attenuation of DF laser radiation is not well defined at present. The 3 to 4 μm region is considered to be an atmospheric window because of relatively low molecular absorption. However, aerosol extinction has been estimated to be comparable to or greater than molecular absorption in this region. Unfortunately the scarcity of data on aerosol optical properties makes these estimates unreliable for systems evaluation, although both scattering and absorption contribute to laser attenuation. It is absorption which affects the onset of such deleterious effects as thermal blooming. Since the threshold for aerosol induced thermal blooming is a function of the aerosol absorption coefficient at the particular wavelength of interest, there is particular interest in the degree of aerosol absorption at DF laser wavelengths.

The program described in this report was designed to measure the total extinction (scattering plus absorption) and the scattering of DF laser radiation by atmospheric aerosols. The data were to yield the corresponding extinction and scattering coefficients, the difference of which is the desired absorption coefficient. Such data would permit an accurate assessment of the role of aerosols in atmospheric attenuation and in degradation of DF laser beam profiles.

An integral part of the program was an extensive effort to characterize the atmospheric aerosols used in the measurements. The aerosols were to be characterized by their chemical composition, particle number density and mass loading. This would provide a means of relating the optical data obtained in this program to aerosols found in other geographic areas.

During the contract period, the experimental facilities necessary for the measurement of the aerosol extinction and scattering coefficients were designed and fabricated. In addition, the measurement technique to determine the total aerosol extinction coefficient was subjected to preliminary calibration tests. These tests indicated that, as originally devised, this measurement technique was subject to experimental inaccuracies which made the data of little value at the low extinction

levels expected for ambient aerosols. The sources of the experimental error were subsequently identified, and modifications to the apparatus were specified which would reduce the experimental error in the data to acceptable levels. Unfortunately, these modifications were devised late in the contract period, and they could not be fully implemented. Consequently, aerosol data could not be acquired.

Section 2 of this report describes the experimental facility fabricated for the program. The theory of the measurement and the equipment designed to perform the measurement are presented for both aerosol extinction and scattering. Calibration procedures are also described. Section 2 concludes with Subsection 2.5 which summarizes the preliminary extinction data obtained with the system, and discusses the inadequacies of the apparatus which prevented measurement of the desired aerosol properties.

2. EXPERIMENTAL INVESTIGATION

2.1 Introduction

The primary objective of the experimental program as described in Section 1 was to determine the absorption coefficient of ambient atmospheric aerosols at DF laser wavelengths. Since the absorption cannot be measured directly, both the aerosol extinction coefficient (absorption plus scattering) and the scattering coefficient were to be measured simultaneously, and the difference of the two taken to obtain the desired result. In the present section, we present a detailed discussion of the theory of the measurements and the apparatus required to obtain the data. The extinction measurement is described in Subsection 2.2, and the scattering measurement is discussed in Subsection 2.3.

2.2 Extinction Measurement

2.2.1 Theory of the Measurement

The extinction coefficient for atmospheric aerosols were to be determined by measuring the attenuation of DF laser radiation as it propagates through a folded-path geometry for a total distance of up to 400m. In this part of the subsection, we describe the theory of the measurements, and the method by which the extinction coefficient, k_{ext}, is determined from the laboratory data. The experimental apparatus, and the calibration techniques are discussed in the succeeding parts of Subsection 2.2.

The laboratory apparatus is shown schematically in Figure 2.1 and photographs of the facility are presented as Figures 2.2 and 2.3. The single-line, diffraction-limited output from a DF TEA laser was focused onto the entrance plane of a 400m White cell. Eighty traversals of a 5m path were used to obtain the total-path length. After passing through the aerosol in the cell, the emerging beam of intensity I was focused onto infrared detector D_4, and produced a voltage V. Ahead of the White cell, the laser beam was sampled with a beam splitter. The reference beam of intensity I_o was focused onto a second detector D_3, and produced a voltage V_o.

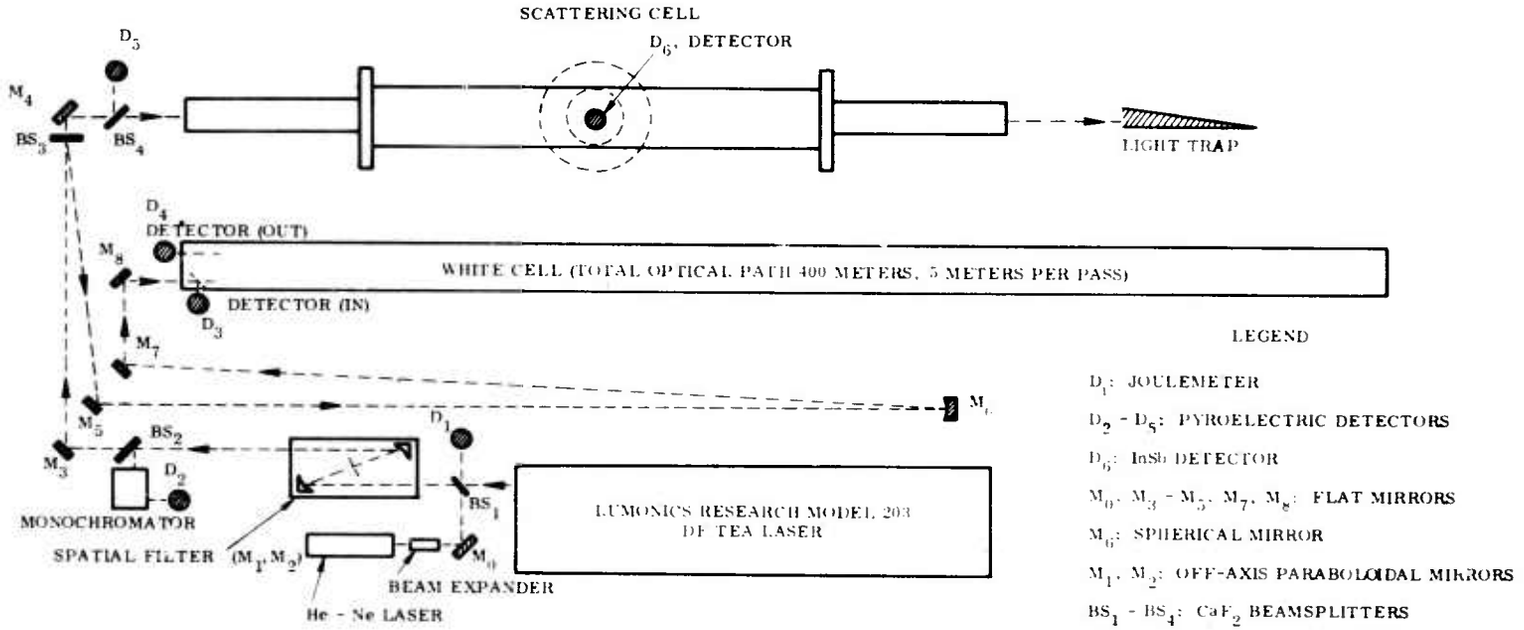

Figure 2.1 - Schematic of Experimental Apparatus.

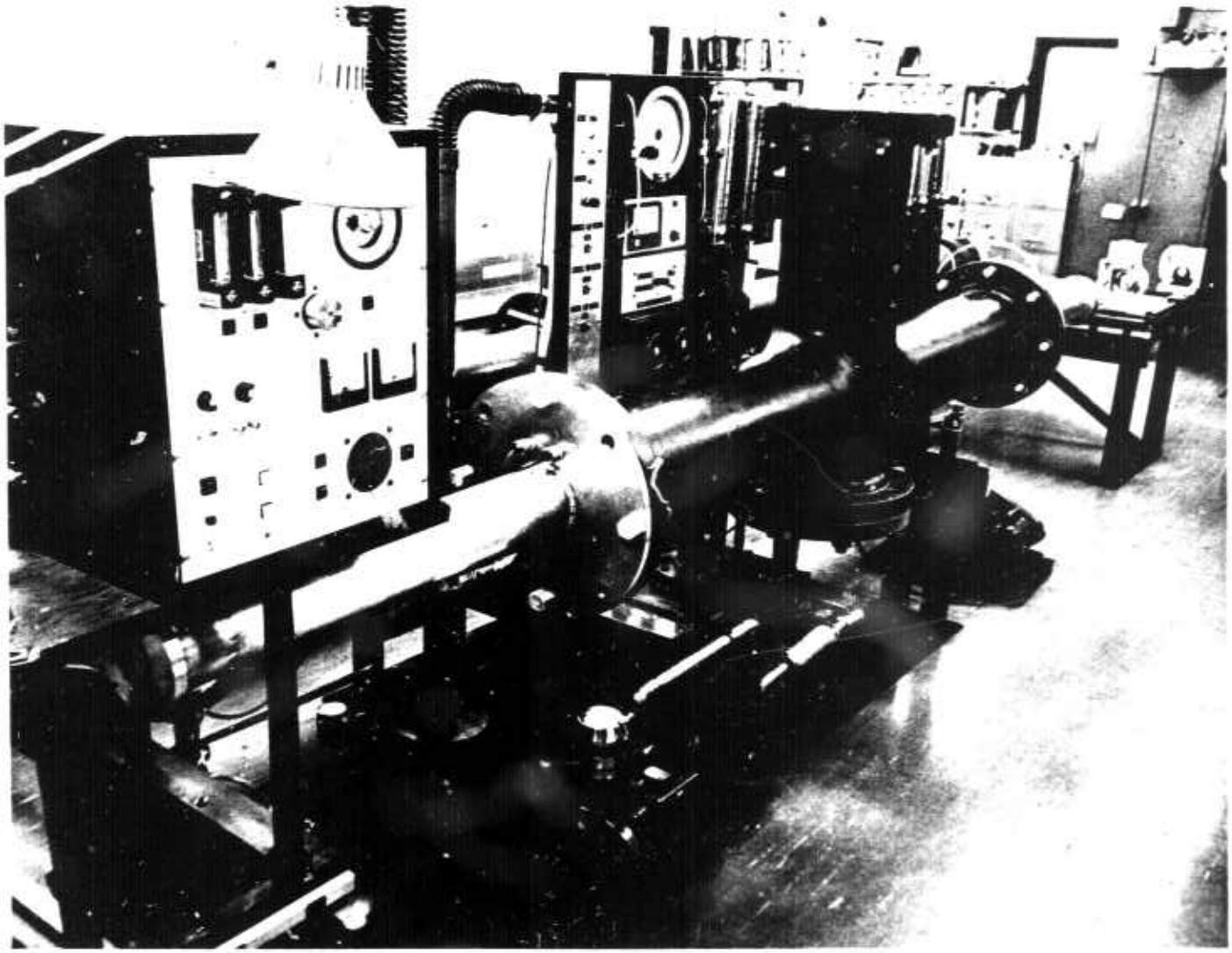

AL-1188

Figure 2.2 - Laboratory Layout of Experimental Measurement: Scattering Cell and Control Panel.

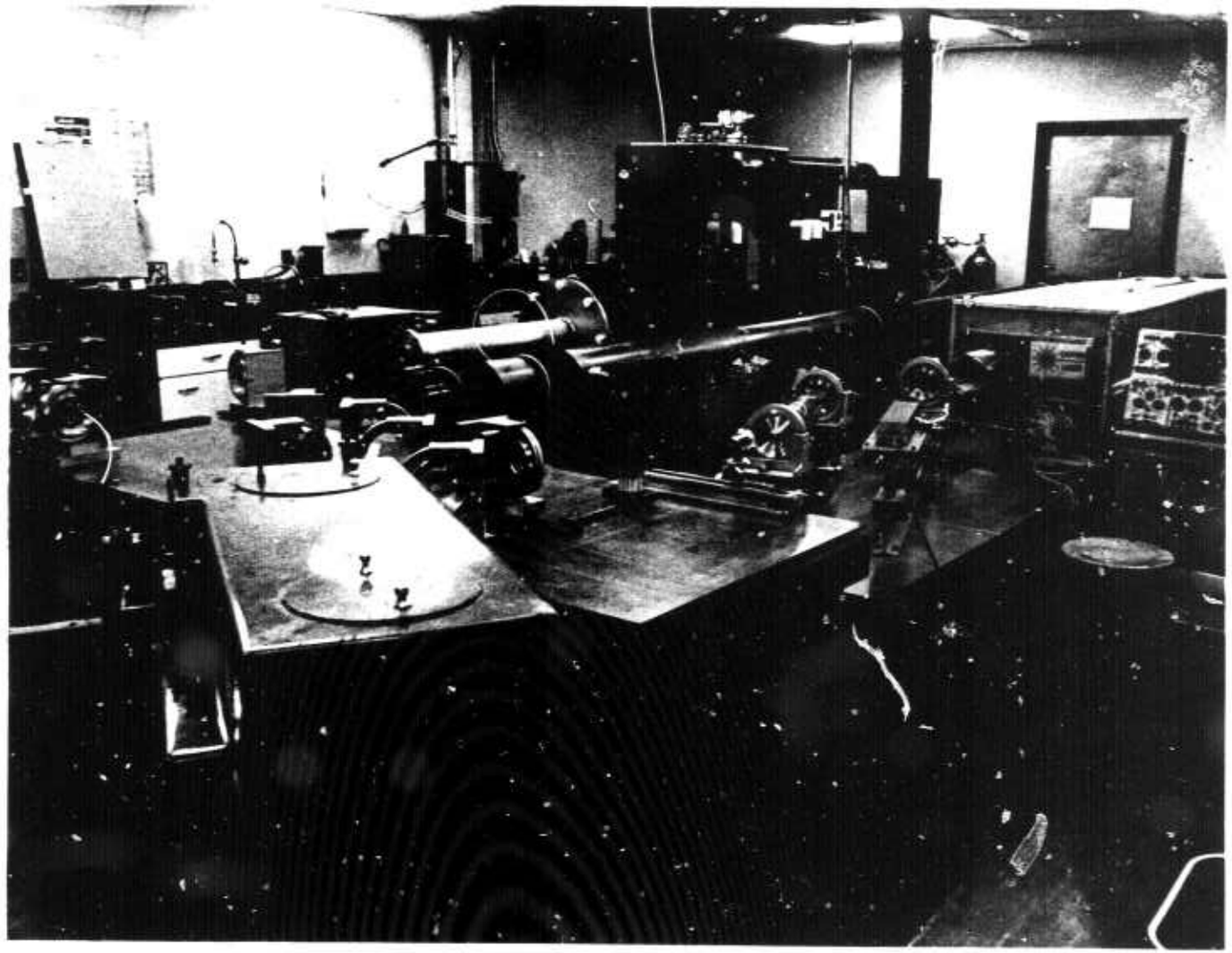

AL-1189

Figure 2.3 - Laboratory Layout of Experimental Measurement: Optics Tables, Laser, and White Cell.

For every microsecond laser pulse, two quantities were measured: the reference intensity I_o and the intensity difference $(I_o - I)$. The extinction coefficient follows from Beer's law

$$I = I_o \exp(-k_{ext} L) \quad . \tag{2.1}$$

This relationship assumes that energy is lost from the beam only by first-order processes such as single absorption and scattering, and not by higher-order effects such as multiple scattering. Single scattering prevails so long as $k_{ext} L < 0.1$. For naturally occurring aerosols, the upper bound on the expected extinction coefficient is 10^{-1} km^{-1}. Thus $k_{ext} L$ was to be, at most, about 10^{-2} in the experiments.

For such small values, it is advantageous to expand the exponential in a power series,

$$\exp(-k_{ext} L) = 1 - k_{ext} L + \frac{(k_{ext} L)^2}{2} - \frac{(k_{ext} L)^3}{3} + \ldots .$$

Retaining the first three terms and rearranging Eq. (2.1) yields

$$\frac{(I_o - I)}{I_o} \simeq k_{ext} L - \frac{(k_{ext} L)^2}{2} \quad . \tag{2.2}$$

For values of $k_{ext} L$ on the order of 10^{-2}, this approximation introduces an error on the order of 10^{-4}. Equation (2.2) forms the basis for determining $k_{ext} L$ in very weakly attenuating systems.

In the experimental arrangement shown in Figure 2.1, the reference signal V_o was set equal to the signal V in the absence of an attenuating medium in the White cell, in which case the output of the differential amplifier was zero, aside from a noise component due to detector-plus-amplifier noise. With an attenuating medium in the White cell, the signal V_o was greater than V, and the differential amplifier output became $V_o - V$.

To determine the aerosol extinction, the difference measurements were to be made in the following three situations: when the absorption cell was 1) empty, 2)

with filtered air, and (3) filled with aerosol-ladened air. This would supply a reference of zero-attenuation, attenuation due to molecular absorption, and attenuation due to molecular absorption and aerosol extinction. In this way, the molecular contribution could be subtracted from the attenuation, leaving only the aerosol contribution.

The apparatus was calibrated by replacing the aerosol in the White cell with a CH_4 - N_2 a gas mixture whose absorption coefficient is well known. This method provided a calibration of the apparatus at the same attenuation levels as expected for the aerosols.

2.2.2 Description of the Optical Train and the White Cell

The DF laser shown in Figure 2.1 was a Model 203 Lumonics TEA laser. Operating in an unstable resonator configuration with a diffraction grating in the cavity, the laser was tuned to give an output consisting of a single line with a superradiant background. In the far field, the signal line constituted the central core of the beam and was diffraction-limited, with a divergence of $\theta_d = 0.15$ mrad. The superradiant background formed satellite rings around the central spot and had a divergence of approximately 1.0 mrad. With spatial filtering, this background was removed, leaving a single-mode, diffraction-limited beam as the usable output from the laser. The beam diameter at the exit of the laser was typically 3.5 cm.

The energy output of the laser was typically 50 mJ per pulse, and varied by ± 5% from shot-to-shot. The temporal width of the pulse was approximately 1 μsec, with an initial spike 0.2-μsec wide, containing approximately 40% of the total pulse energy.

The spatial filter shown in Figure 2.1 consisted of two aluminum coated, 18^o off-axis paraboloids purchased from the Perkin Elmer Corporation. Indicated as M_1 and M_2 in the figure, these mirrors had a 312 mm (12.3 in.) focal length, and a 68 x 70 mm clear aperture. The blur circle was quoted to be 0.002 in. (0.05 mm).

The aperture in the filter was a pinhole supplied by Optimation, Inc. It consisted of an aperture 1 mm in diameter drilled in a 0.375 in. diameter stainless steel substrate, 0.001 in. thick. With the parabolic mirrors described above, this corresponded to a 3 mrad system.

To avoid laser breakdown in the vicinity of the focal volume of the spatial filter, the pinhole was placed in a 2.5 in. diameter cylindrical vacuum chamber 6 in. in length. The chamber was fitted with sapphire windows and was capable of holding a vacuum of 0.1 to 1.0 torr.

The laser beam emerging from the spatial filter was diffraction limited and approximately 3.5 cm in diameter. The beam was directed by three flat mirrors, M_3, M_4, and M_5 in Figure 2.1, onto a 7.6 cm diameter, 5m focal length spherical mirror M_6. This mirror effectively matched the f-number of the beam to that of the White cell (f/150). With the aid of two additional flats, M_7 and M_8, the spherical mirror focused the laser beam onto the 1.5 mm entrance aperture of the cell.

Mirrors M_3 through M_8 were supplied by PTR Optics, Inc., and they consisted of a silver-coated pyrex substrate with a thorium fluoride overcoat. The mirrors were quoted to be flat to $\lambda/10$ in the visible.

The aerosol extinction coefficient was to be determined by measuring the attenuation of the laser intensity as the beam traverses 80 passes in the White cell. The cell was an 8 in. diameter 6m long aluminum tube with three aluminum coated spherical mirrors mounted internally. The cell was designed and fabricated by Dr. John U. White of the White Development Corporation, Stamford, Conn. to yield a diffraction limited after 20 passes. The transmission through the cell exceeded 75% after 20 passes.

Provision was made for dry nitrogen gas to flow over the mirrors to prevent these mirrors from coming in contact with the working medium in the cell. Thus, the quality of the mirrors would not degrade with time due to dust collecting on the optical surfaces. The "gas windows", however, limited the effective optical path in the cell to 5m per pass.

Focusing optics required for detectors D_3 or D_4 were 5 cm diameter, 25 cm focal length spherical mirrors (not shown in Figure 2.1). The beam diameter at the focal plane was 1.5 to 2.0 mm for the f/150 system, while the detector size was 2 mm diameter.

The alignment of the White cell, as well as the entire optical system, was performed with the assistance of the Spectra Physics, Model 155 He-Ne laser shown in Figure 2.1. The output from this 0.5 mw CW laser was passed through a beam expander to match the beam diameter and divergence to those of the DF laser. The

0.6328 μm beam was then made collinear with the DF beam with the use of a turning flat, M_0, and a CaF_2 beamsplitter, BS_1. Since the optical system contained no refractive elements (excluding the spectrometer), it was ideally suited for alignment with the visible beam.

The spectrometer shown in Figure 2.1 was a used to calibrate the diffraction grating located inside the laser cavity.

2.2.3 Detection System

The detectors used in the extinction measurement, D_3 and D_4 in Figure 2.1, were Model kT-1120S pyroelectric detectors manufactured by Laser Precision, Inc. Each unit was supplied with a Model kTM-333 preamplifier and a Model kTM-900 fixed load resistor. The active element size was 2.0 mm diameter. The electronic characteristics for each detector are listed in Table 2.1. Although each unit was also supplied with a variable load up to $10^{10}\Omega$, only the fixed load corresponding to a 10 MHz bandwidth is listed. The recommended maximum output from these detectors is approximately 1.0v. At higher output levels, the detectors approach their saturation levels.

TABLE 2.1 CHARACTERISTICS OF LASER PRECISION, INC., kT-1120S PYROELECTRIC DETECTORS, WITH kTh-333 PRE-AMPLIFIERS AND kTM-900 FIXED LOAD MODULES

Detector	Current Responsivity (μamp/w)	Capacitance (pf)	Load Resistor (Ω)	Voltage Responsivity (v/w)	RC Time Constant (nsec)
D_3	1.51	53.1	270	4.08×10^{-4}	14.3
D_4	1.23	74	200	2.46×10^{-4}	14.8

The electronics used with these detectors are outlined in Figure 2.4. The output from each kT-1120S/kTH-333 detector-amplifier unit was fed into an Analog Devices, Inc., Model 50K wideband amplifier. This acted as a buffer amplifier to null the difference measurement when no absorber was in the White cell. The output from each buffer was fed into a Tektronix, 1A5 differential amplifier which performed the

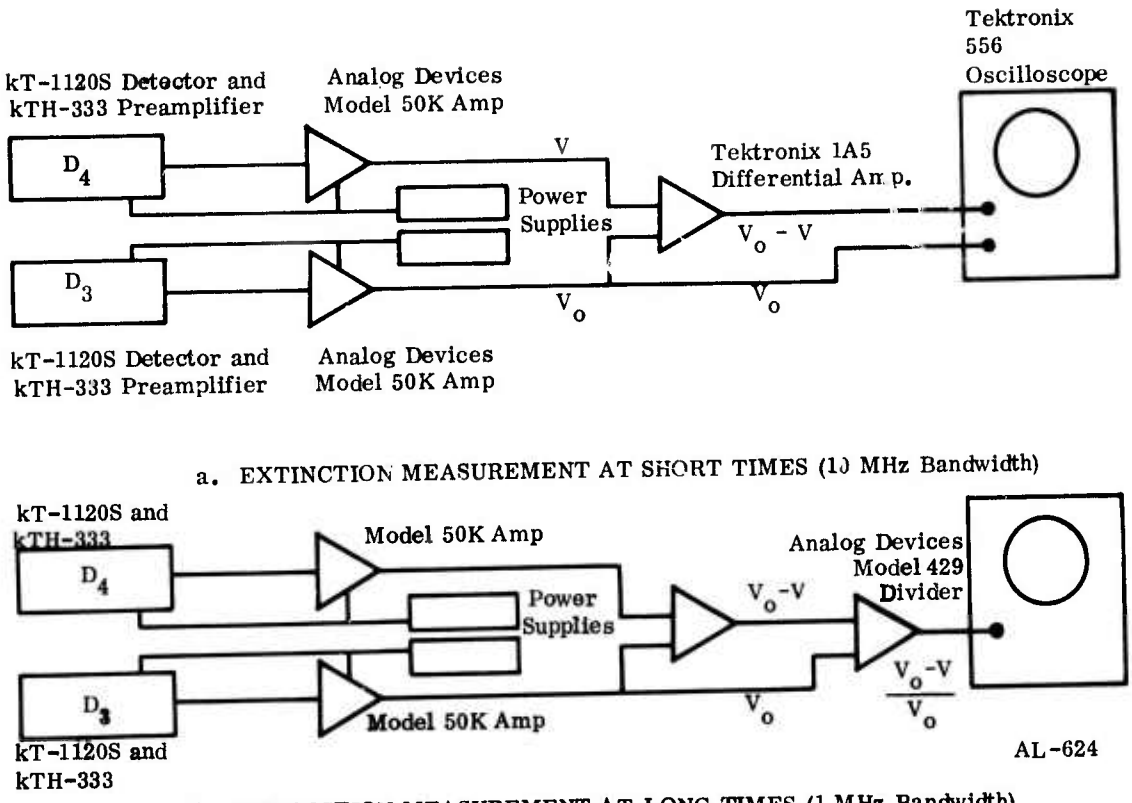

Figure 2.4 - Schematic of Electronics for Extinction Measurement.

differencing $(V_o - V)$. Here V_o is the reference voltage from D_3, and V is the signal voltage from D_4. The signal $(V_o - V)$ was then displayed on the Tektronix, 556 dual-beam oscilloscope. The reference signal V_o was also displayed on the oscilloscope so that for every laser pulse, the traces could be read and the ratio $(V_o - V)/V_o$ could be determined.

Besides D_3 and D_4, two auxiliary detectors were employed in the system during the extinction measurement. Detector D_2, shown in Figure 2.1, was a Laser Precision, Inc., kT-1120S detector with a kTH-333 preamplifier and a kTM-900 fixed load module. This detector was used in conjunction with the spectrometer to monitor the spectral content of the laser pulse.

In addition, detector D_1 was a Gen-Tec, Inc., Model ED-200 joulemeter that measured the energy in each laser pulse. Detectors D_1 and D_2 provided sufficient diagnostics to monitor the performance of the laser during the measurements.

2.2.4 Aerosol Handling System

An external view of the White cell is shown schematically in Figure 2.5. The entrance and exit ports for the aerosol and the dry N_2 were surrounded by plenum chambers to ensure uniform radial flow. The aerosol was to be introduced into the cell through the plenum chamber at the center of the cell. Inside the plenum chamber, the aerosol would flow into the White cell through eight sample inlet holes equally spaced around the circumference of the cell. The inlet ports for the dry N_2 used for the "gas window" were enclosed in the plenum chambers located at each end of the White cell. The exhaust ports for both the aerosol and the dry N_2 were inside the remaining two plenum chambers.

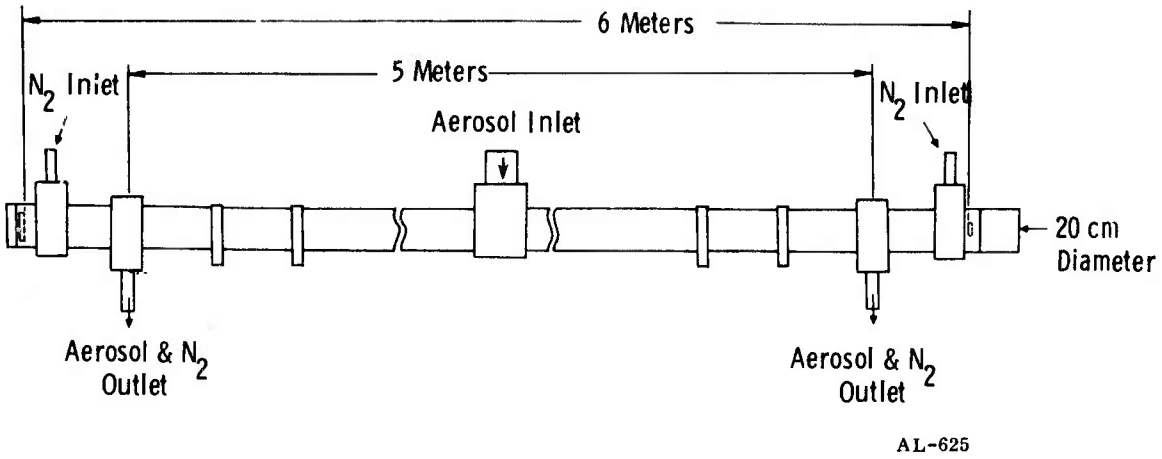

Figure 2.5 - External View of 400m White Cell.

The aerosol was to be drawn from the roof of the building down through the system by means of a blower located downstream of both the White cell and the scattering cell. A schematic of the aerosol and gas handling systems is shown in Figure 2.6. The flow of aerosol through each cell was to be monitored and balanced using standard flow meters. This is especially important in the operation of the White cell where the aerodynamic window flow must be matched to the aerosol flow. Maximum flow rate was 94 liter/min, corresponding to an aerosol residence time of 0.9 min in the White cell.

The meteorological conditions at the time the aerosol was sampled were to be monitored by a Heathkit, Model ID-1290 weather station. This instrument provided the wind speed and direction at the point where the aerosol was to be drawn into the building, approximately 10 ft above the roof. The barometric pressure and both the outdoor and indoor temperatures were also recorded.

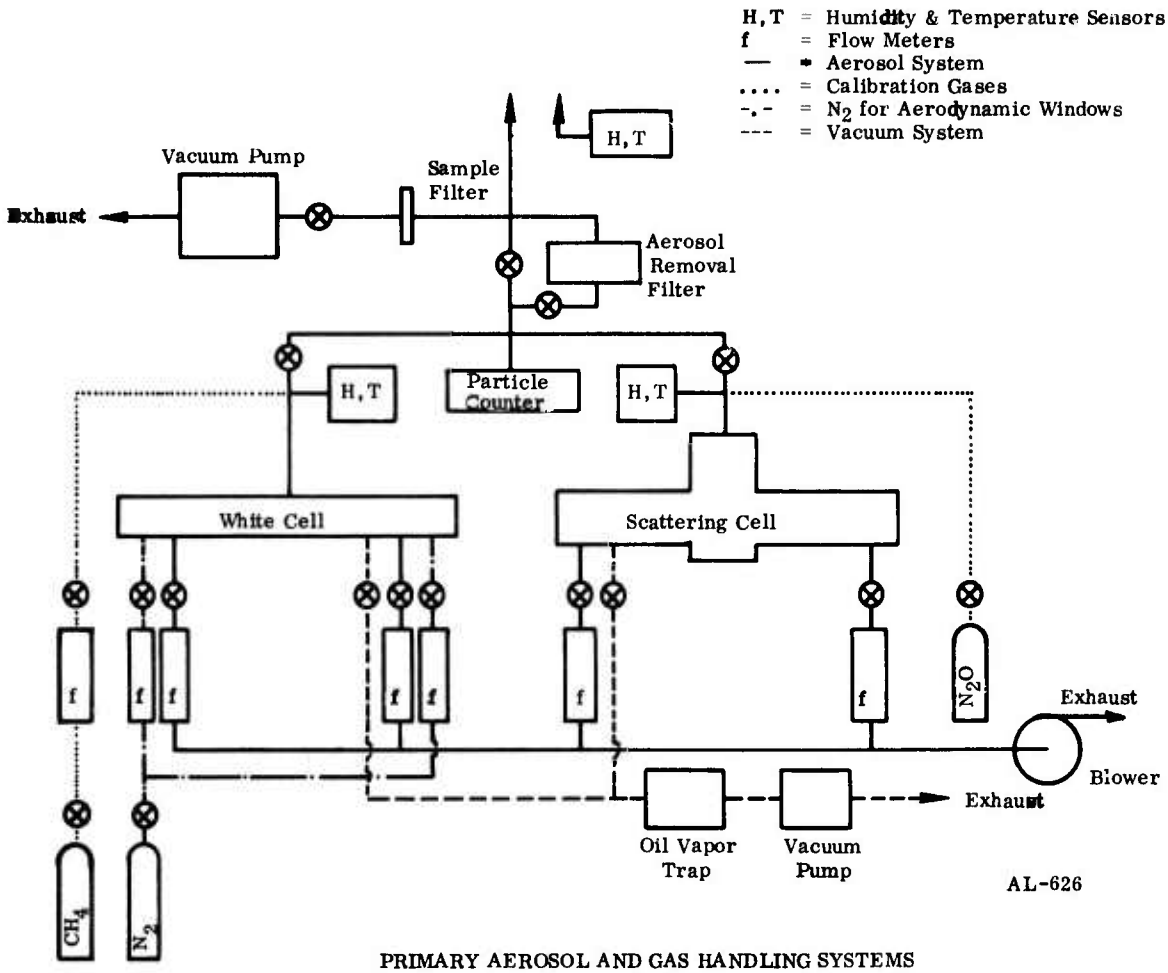

PRIMARY AEROSOL AND GAS HANDLING SYSTEMS

Figure 2.6 - Primary Aerosol and Gas Handling Systems.

The water content in the atmosphere was to be measured with a Yellow Springs Instrument Company, Model 91HC dew point hydrometer. The lithium chloride sensors were placed on the roof where the aerosol was to be sampled and at the entrance port of the White cell and the scattering cell in the laboratory. Finally, the temperature of the aerosol-laden air was to be monitored with a Yellow Spring Instrument Company, calibrated thermistors located on the roof and in each cell. These sensor locations are indicated by H, T in Figure 2.6.

2.2.5 Calibration Procedure

To establish the validity of the data and to determine the measurement accuracy, a thorough calibration procedure had to be followed. Outlined in the present section is a dynamic calibration which would have allowed a direct comparison of the measured aerosol extinction coefficient with the absorption coefficient of a gas as measured in other laboratories.

In essence, the dynamic calibration was an attenuation measurement with the White cell filled with a gas whose absorption coefficient is known at the DF laser line. The choice for this application was CH_4. As with the aerosol measurements, the first step in the calibration was to take data when the White cell was empty. This determined a zero reference, and ensured one of the fact that the measured voltages could be related to the extinction coefficient by Eq. (2.2) or by

$$\frac{V_o - V}{V_o} = 1 - \beta \exp(-k_{ext} L) \simeq 1 - \beta \left[1 - k_{ext} L + \frac{1}{2} (k_{ext} L)^2 \right] .$$

Here, β is a constant which accounts for the reflectivity of the mirrors, the presence of beamsplitters in the optical train, and for the (constant) difference between the responsivity of the two detectors. Nulling the signal with an empty cell simply guarantees that $\beta = 1$.

When the null measurement was completed, the White cell was filled to one-atmosphere pressure with a CH_4 - N_2 gas mixture. The absorption coefficient for CH_4 in N_2 at 298°K is shown in Figure 2.7 as a function of CH_4 partial pressure. The values shown apply to the center of the $P_2(8)$ line of DF, and are values measured recently by Spencer.[1]

The corresponding attenuation by CH_4 at the center of the $P_2(8)$ line is also shown in Figure 2.6 for a 400m path length. For CH_4 partial pressures in the range of 10^{-5} to 10^{-3} atm, the CH_4 - N_2 mixture provided the same attenuation expected by aerosols. Therefore, a successful dynamic calibration would verify that the entire system was operating properly at the desired sensitivity.

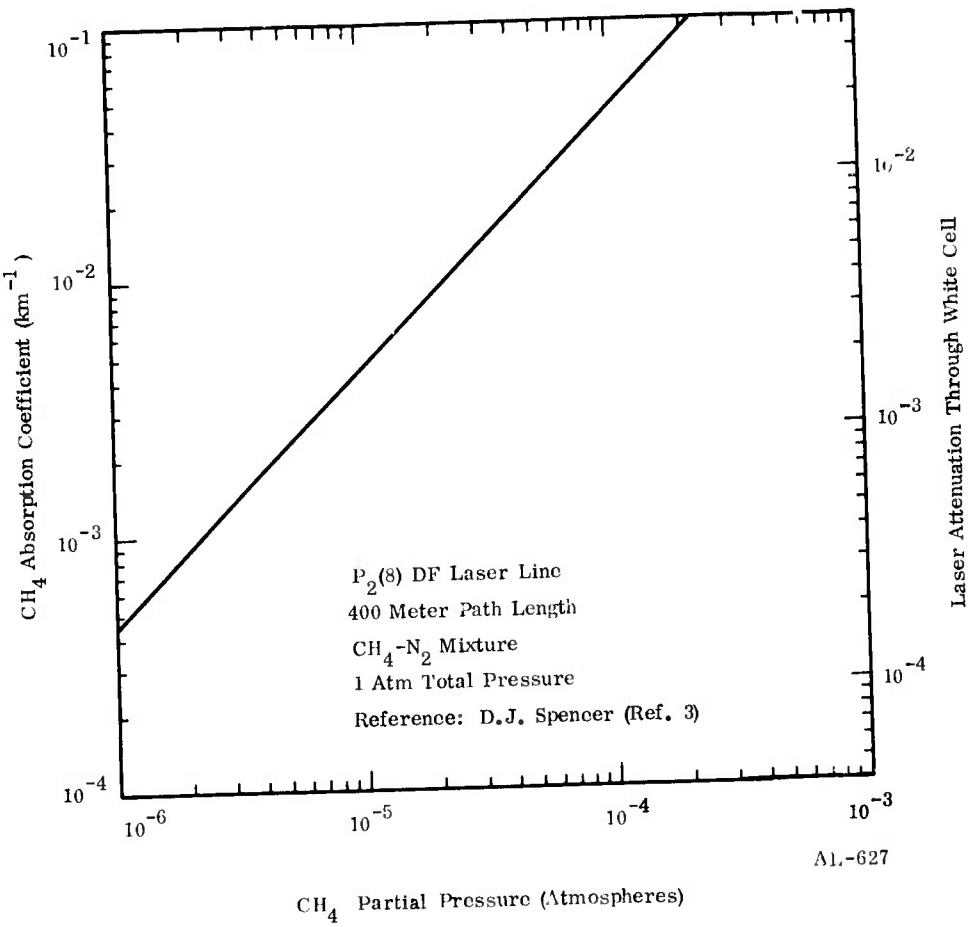

Figure 2.7 - Calibration for Extinction Measurements. Attenuation by CH_4.

This calibration, performed at several laser lines, would achieve the additional goal of measuring the exact optical path in the White cell. This path length depended critically upon the location of the interface between the absorbing medium and the dry N_2 from the gas windows. Therefore, the path length had to be determined under the flow conditions to be employed in the aerosol measurements.

2.3 Scattering Measurement

2.3.1 Theory of the Measurement

The scattering coefficient of the atmospheric aerosol was to be determined from a measurement of the intensity of radiation scattered out of a parallel laser beam as the beam traversed a 4.5m cell containing the aerosol. An infrared detector was to be placed several centimeters from the axis of the laser beam and would monitor the scattered radiation with a field-of-view of approximately 170^{o}. A schematic of the region around the detector is shown in Figure 2.8.

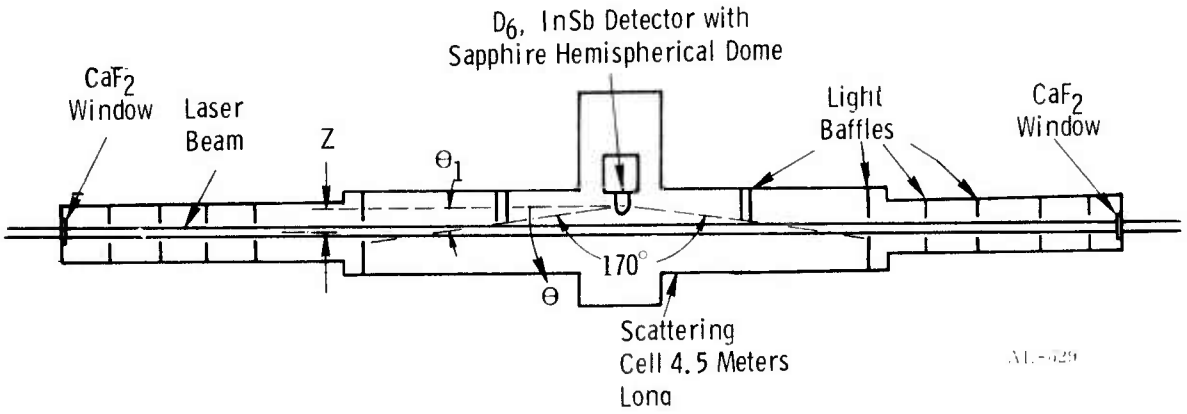

Figure 2.8 - Schematic of Aerosol Scattering Cell.

The experimental arrangement for the scattering measurement was straightforward, and it permitted one to obtain a direct measurement of the scattering coefficient in a single laser pulse if stray background radiation had been properly suppressed. This can be shown by calculating the signal for the arrangement shown in Figure 2.8. Let the beam intensity be I_o w/cm^2 and the beam area be A_B. The detector has an area A_d, and is placed at a distance Z from the beam. The signal that one observes is given by the relation

$$P_{scat} = \int_o^{\infty} \int_V I_o \, n(r) \, \sigma \, (r,\theta) \quad \Omega_d \, dV \, dr \quad . \tag{2.3}$$

The integration is over the volume V occupied by the laser beam, and over the particle size distribution, n(r). In Eq. (2.3), r is the particle radius; σ is the scattering cross section, a function of r and θ; and Ω_d is the solid angle of the detector, as seen from the volume element dV. If x is the coordinate along the beam, then $dV = A_B\, dx$. The total beam power can be written as $P_o = I_o A_B$, and the detector solid angle is

$$\Omega_d = \frac{A_d \sin\theta}{x^2 + Z^2} \quad . \tag{2.4}$$

The factor $\sin\theta$ transforms the detector area to the project area seen from the volume element dV. Inserting these expressions into Eq. (2.3) yields

$$P_{scat} = P_o \int_o^{\infty}\int_{-\infty}^{\infty} n(r)\, \frac{\sigma(\theta,r)\, A_d \sin\theta}{x^2 + Z^2}\, dx\, dr \quad . \tag{2.5}$$

By using the relation $x = Z \text{ cotan } \theta$ to transform from the x- to the θ-coordinate, the signal becomes

$$P_{scat} = \frac{P_o A_d}{Z} \int_o^{\infty}\int_o^{\pi} n(r)\, \sigma(\theta,r) \sin\theta\, d\theta\, dr \quad . \tag{2.6}$$

Since the scattering cross section is related to the scattering coefficient, k_{scat}, by

$$k_{scat} = 2\pi \int_o^{\infty} dr \int^{\pi} \sin\theta\, n(r)\, \sigma(r,\theta)\, d\theta \quad , \tag{2.7}$$

one obtains a relation between the signal and the scattering coefficient,

$$P_{scat} = \frac{P_o A_d}{2\pi Z}\, k_{scat} \quad \text{watts} \quad . \tag{2.8}$$

In the ideal case described by Eqs. (2.6) and (2.8), the beam would be observed from $x = -\infty$ to $x = +\infty$, or for the range of angles from $\theta = 0^o$ to $\theta = 180^o$. However, this cannot be achieved in the laboratory because the radiation scattered from the side walls and end plates would be seen by the detection system. Instead, baffles limited

the range of viewing angles from θ_1 to $(180^o - \theta_1)$, precluding observations of forward and backward scattering. This corresponded to offsetting the detector by the distance Z = 5.3 cm and 11 cm from the beam for $\theta_1 = 10$ and 20^o, respectively. This distance had to be short in order to minimize θ_1.

Most of the ambient aerosol particles are contained in the size range less than 1 μm. The scattering cross section $\sigma(\theta, r)$, on the assumption of spherical aerosol particles, was expected to be only a weak function of scattering angle θ, so that $\sigma(\theta, r) \sim \cos^2\theta$ was a good approximation. Since the scattering cross section does not peak strongly at 0 and 180^o, the errors involved in the truncation were not serious, approximately 10 and 17% for $\theta_1 = 10$ and 20^o, respectively. Thus, a good measurement could be obtained even without observing the forward and backward directions.

The scattering coefficient is obtained by solving Eq. (2.8),

$$k_{scat} = \frac{2 \; Z \; P_{scat}}{P_o \; A_d} \quad . \tag{2.9}$$

2.3.2 Description of the Apparatus

The experimental apparatus for measuring the atmospheric aerosol-scattering coefficient is shown in Figure 2.1. A beamsplitter directed only a small portion of the laser radiation to the White cell. The major portion of the beam (~90%) passed through the scattering chamber. The chamber was a tube 30 cm in diameter and 4.5m long, with the laser beam propagating along its axis. Annular disc diaphragms were placed in the tube to suppress radiation scattered from the walls (see Figure 2.8). A Santa Barbara Research indium antimonide infrared detector was located equidistant from the ends of the chamber to maximize the distance to the end windows. The detector, 2.0 mm in diameter, was placed several centimeters away from the beam, and observed radiation scattered from the medium. The detector was fitted with a sapphire hemispherical dome to minimize reflection losses at the detector window for rays striking the detector at shallow angles of incidence.

The photovoltaic detector was liquid nitrogen cooled and had a D* of 2.4×10^{10} 2.4×10^{10} cm-Hz$^{1/2}$/w at 3.8 μm. This corresponded to a NEP of 2.3×10^{-8} w for a 10 MHz bandwidth.

Baffles placed near the detector eliminated the stray light scattered from the walls of the chamber and from the windows in the end walls. The disc baffles closest to the detector were 1m away on each side. These discs performed the major baffling of the light, while inner secondary baffles on the detector side removed the light scattered from the closest discs.

The reference intensity for the scattering measurement was to be determined by detector D_5 shown in Figure 2.1. This was a Laser Precision, Inc., Model kT-1520S pyroelectric detector with a 2 mm diameter element. The detector's capacitance was 25 pf, and current responsivity of 1.66 μamp/w. For 50Ω load, this corresponded to an RC time constant of 12.5 nsec and a voltage responsivity of 8.3×10^{-5} v.w. For a 10 MHz bandwidth and a 50Ω load, the self-noise was $e \times 10^{-6}$v or 0.036w.

Approximately 10% of the laser intensity was directed onto D_5 by a CaF_2 beam-splitter, BS_4, located in front of the entrance to the scattering cell. As for the detectors used in the extinction measurement, detectors D_5 and D_6 were aligned with the assistance of the He-Ne laser.

As for the White cell, the aerosol was to flow through the scattering cell during the measurement. Coming from the same manifold which supplies the White cell, the aerosol was to enter the scattering cell at the center near detector D_6, and flow out of the cell at each end. Flowmeters at the exit ports were to control the flow rate. As mentioned in Subsection 2.2.4, the temperature and water vapor content were to be monitored inside the cell.

2.3.3 Calibration Procedure

In order to perform measurements of absolute scattered intensities, one must determine the solid angle and sensitivity of the detector, the gain of the electroncis, and the beam diameter and power density of the laser. In principle, these quantities could be calculated, determined from manufacturers' specification, or in the case of the laser power, measured in the laboratory. Alternatively, if a source of known intensity at 3.8 μm were available which has the same geometric shape as the scattering volume, then the measurement of the signal strength from this source would yield an overall responsivity of the detection system. This responsivity would contain all the unknown factors in the system, and would eliminate the need for the error-prone analysis indicated above.

An example of such a source is the 3.8 μm fluorescence from a known molecular system following absorption of DF laser radiation. In this case, the same DF laser would be used so that the source geometry would be identical to that for the scattering measurement. Moreover, if the fluorescence measurement were performed in the first few microseconds following the laser pulse, then the calibration would be carried out over a time scale comparable to that for the scattering measurement.

In the present system, resonance fluorescence from pure N_2O was to be used in the calibration. The absorption coefficient for N_2O has been measured previously[1] at several DF laser lines. The data indicate that at the $P_2(11)$ ($\lambda = 3.9155$ μm) and the $P_3(8)$ ($\lambda = 3.9272$ μm) laser lines, absorption by N_2O is strong enough to permit the calibration to be performed at gas pressures in the range of 50 to 200 torr. At these levels, collisional quenching of $N_2O(20^00)$, the upper level in the absorption process, is insignificant during the laser pulse. Consequently, at the end of the pulse, the population of the radiating state is given by

$$\left[N_2O(20^00)\right] = \left[N_2O(00^00)\right] \sigma_r \frac{E_o}{A_B} \left(\frac{\lambda}{hc}\right) \exp(-t/\tau)$$

$$= k_r \frac{E_o}{A_B} \left(\frac{\lambda}{hc}\right) \exp(-t/\tau) \quad . \tag{2.10}$$

Here σ_r and $k_r = \left[N_2O(00^00)\right] \sigma_r$ are the absorption cross section and absorption coefficient, respectively, E_o is the laser pulse energy, and hc/λ is the laser photon energy. The quantity τ is the time constant for the relaxation of the $N_2O(20^00)$ both by collisions (τ_o) and radiative decay (τ_r). Thus, $\tau^{-1} = \tau_o^{-1} + \tau_r^{-1}$. The time t is measured from the end of the laser pulse.

In the measurement geometry shown in Figure 2.9, the InSb detector was oriented 90^o to the laser axis and had a field-of-view of approximately 170^o, i.e., $\theta_1 \simeq 5^o$. Under these conditions, the N_2O emission is given by

$$P_{N_2O} = \int_{Vol} \frac{\left[N_2O(20^00)\right]}{\tau_r} \frac{hc}{\lambda} \frac{\Omega_d}{4\pi} \, dVol \tag{2.11}$$

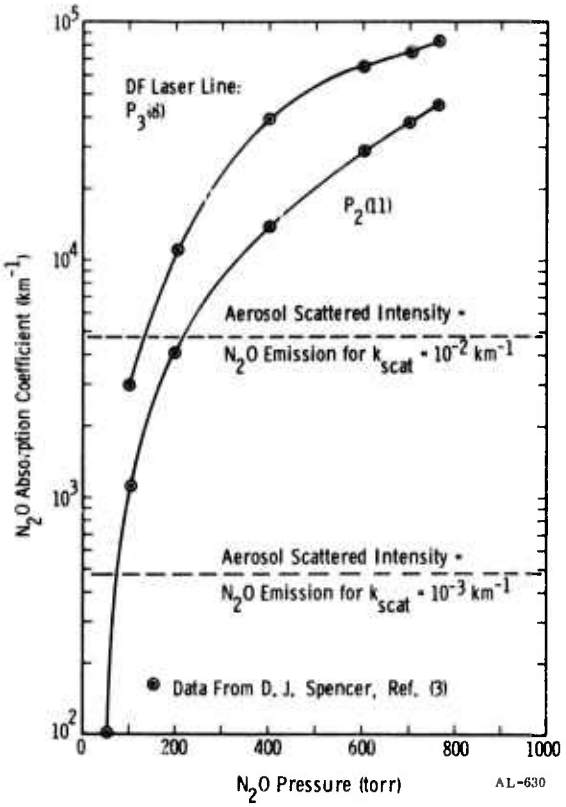

Figure 2.9 - N_2O Absorption Coefficient and Operating Levels for Scattering Calibration.

where the integration is performed over the gas volume irradiated by the laser beam. Expressing solid angle and the volume element in terms of x, θ, and Z, one can evaluate the integral and obtain for the N_2O emission incident on the detector

$$P_{N_2O} = \frac{\left[N_2O(20^00)\right]}{\tau_r} \frac{hc}{\lambda} \frac{A_B A_d}{2\pi Z} \quad . \tag{2.12}$$

With Eq. (2.13), the fluorescence signal strength can be expressed as

$$P_{N_2O} = \frac{k_r}{\tau_r} \frac{E_o A_d}{2\pi Z} \exp(-t/\tau) \quad \text{watts} \quad . \tag{2.13}$$

Therefore, the calibration intensity is a simple function of the measurable parameters E_o, A_d, and Z, and of the radiation parameters k_r and τ_r.

As mentioned above, k_r has been determined in other laboratories. The radiative lifetime, τ_r, can be calculated directly from previous band intensity measure nents,[2] and is found to be $\tau_r = 133$ msec for the $N_2O(20^00) - (00^00)$ band at 3.90 μm. The rate constant for collisional deexcitation of $N_2O(20^00)$ in pure N_2O is estimated to be $k_c \simeq 10^{-14}$ cm^3-sec^{-1}, so that the time constant for collisional quenching is

$$\tau_c \simeq -\frac{4 \times 10^{-6}}{p_{N_2O}} \quad \text{sec} \quad ,$$

where P_{N_2O} is the gas pressure in atmospheres. Therefore, the time constant in Eq. (2.13) is given by $\tau \simeq \tau_c$. For $50 \leq p_{N_2O} \leq 200$ torr (i.e., $0.066 \leq p_{N_2O} \leq 0.263$ atm), τ assumes values in the range of $15 < \tau < 60$ μsec. Consequently, during the measurement of the N_2O fluorescence ($0 \leq t \leq 2$ μsec), collisional quenching is insignificant, and the signal strength may be approximated by

$$P_{N_2O} \simeq \frac{k_r}{\tau_r} \; -\frac{E_o A_d}{2\pi Z} \quad \text{watts} \quad . \tag{2.14}$$

This analysis applies to the measurement conditions provided the N_2O gas pressure is chosen so that saturated absorption is avoided. This condition is satisfied if

$$2 \sigma_r \delta \Phi < 1 \quad , \tag{2.15}$$

where $\sigma_r = k_r \Big/ \left[N_2O(00^00; J)\right]$ is the absorption cross section, $\delta = \left[N_2O(00^00; J)\right] \Big/ \left[N_2O(00^00)\right]$ is the ratio of the population in the lower absorbing level to that in the levels strongly coupled to the absorbing level, and Φ is the total laser photon flux in photons/cm^2. In the expression for δ, J is the rotational quantum number of the absorbing level. For the scattering measurement, the laser pulse energy was 50 mJ and the beam diameter in the scattering cell was 3.5 cm, so that $\Phi \simeq 10^{17}$ photons/cm^2. The quantity $2\sigma\delta$ then reduces to

$$2 \sigma \delta \Phi = 8 \times 10^{-3} P_r$$

at 300°K. Here, $P_r = k_r/p_{N_2O}$ is the spectral absorption coefficient in cm^{-1} atm^{-1}. The inequality in Eq. (2.15) requires that $P_r < 125$ cm^{-1} atm^{-1} to avoid nonlinear saturation effects. Spencer's data[1] for N_2O absorption coefficients at the DF laser lines show that this requirement was satisfied at all the intense laser lines for all N_2O gas pressures of interest (i.e., ≤ 1 atm).

The ratio of the aerosol scattered intensity to the N_2O fluorescence obtained from Eqs. (2.8) and (2.14) is

$$\frac{P_{scat}}{p_{N_2O}} = \frac{P_o}{E_o} \; k_{scat} \; \frac{\tau_r}{k_r} \quad . \tag{2.16}$$

Setting $P_o = P_M$, where P_M is the peak laser power given in Subsection 2.2.6 as 3.5×10^6 E_o watts, this becomes

$$\frac{P_{scat}}{P_{N_2O}} = 4.7 \times 10^5 \; \frac{k_{scat}}{k_r} \quad . \tag{2.17}$$

The N_2O absorption coefficients as measured by Spencer at the $P_2(11)$ and $P_3(8)$ DF laser lines are shown in Figure 2.9. Also indicated are the points at which $P_{scat} \simeq P_{N_2O}$ for $k_{scat} \simeq 10^{-3}$ km^{-1} and 10^{-2} km^{-1}. This essentially defined the N_2O pressure range at which the calibration were to be run.

This procedure could also be run at other DF laser lines for which there is substantial N_2O absorption. The $P_2(10)$ and $P_3(7)$ lines were obvious candidates. The selection of the particular line to be used was to be determined by the choice of laser lines for the scattering measurement. Approximately eight laser lines were of sufficient intensity for the scattering measurements, and at least four of these are absorbed by N_2O.

2.4 Aerosol Characterization

Measurements were to be conducted to determine the composition and characteristics of the aerosol used in the experiments described above with a two-fold purpose: first, to identify the contributions of various aerosol sources to the ambient aerosol so

that the results of these studies may have more than local relevance; and second, to monitor changes in the ambient aerosol from the roof-mounted sampling inlet to the scattering and extinction cells.

Aerosol source identification was to combine an elemental analysis of impacted aerosol samples with local and regional wind conditions to determine the nature of the measured aerosol. Major components of the ambient aerosol are expected to be soil dust and sea salt, the so-called continental aerosol, combined with fuel oil ash generated by the widespread use of oil in residential heating systems. The close proximity to a heavily use freeway will also give rise to automobile exhaust aerosols.

Analyses of chemical element composition and total aerosol mass loading were to be performed by Skinner and Sherman Laboratories of Boston. Samples were to be collected by impacting the aerosol on 90 mm diameter Millipore filters of 0.1 and 0.45 μm diameter pore sizes. The sampling times needed to collect above 1 mg were 8 and 0.9 hr, respectively. The larger pore filter is in common use for aerosol studies; however, it was felt that the smaller pore filter will provide a check on the contribution and effects of the more numerous smaller particles.

Source identification was to be accomplished by the method of chemical element balance. In this method, the observed aerosol elemental concentration is compared with concentrations emanating from known sources. The result is a characterization of the aerosol in terms of identifiable constituents. Mathematically, if X_i is the measured concentration of element i and Z_{i_j} is the percent of element i due to source j, then the problem is reduced to solving a set of i equations of the form:

$$X_i = \sum_j Z_{i_j} m_j \qquad (2.21)$$

for the coefficients m_j which represent the mass of material from source j contained in the aerosol. Obviously, the determination of an accurate source matrix (Z_{i_j}'s) is essential. Table 2.2 represents the best available literature values.[3]

Published elemental compositions from samples collected at MIT[4] (Urban Boston) have been analyzed to illustrate the method. Table 2.3 gives the concentrations of key elements. The chemical element balance, using the source coefficients from Table 2.3, gives a set of eight equations in four unknowns. The solutions are:

TABLE 2.2 - SOURCE MATRIX OF KEY ELEMENTS CONCENTRATIONS

Element	Aerosol Source			
	Sea Salt	Soil Dust	Auto Exhaust	Fuel Oil
Na	30.6	2.5		5
Mg	3.7	1.4		0.06
Al		8.2		0.8
Cl	55		6.8	
V		0.006		7
Mn		1.1		0.06
Fe		3.2	0.4	6
Br	0.19		7.9	
Zn		0.006	0.14	0.02

TABLE 2.3 - METROPOLITAN BOSTON AEROSOL
(Source: Gorden, et al., 1974)

Element	Concentration (ng/m^3)
Na	1480
Al	1630
Cl	590
V	980
Mn	30
Fe	1480
Br	224
Zn	260
	Total Observed = 8737 ng/m^3

Soil Dust	55%
Fuel Oil Ash	41%
Sea Salt	3%
Automobile	1%

These results seem compatible with the windy, winter conditions prevailing during the collection.

Atmospheric aerosols are highly hygroscopic with resultant rapid size increase at relative humidities greater than 70 - 80%. Humidity and temperature measurements were to be made at the sampling stack entrance and in each experimental cell.

A portable Royco aerosol particle counter was obtained on loan from Air Force Weapons Laboratories (AFWL). It was to be used to provide relative particle concentrations during the course of these experiments as well as to check for possible aerosol concentration changes between the sampling stack entrance and the experimental cells.

2.5 Results

The program plan called for the fabrication of the White cell and the scattering cell, installation of these in the laboratory, alignment of the optical train as shown in Figure 2.1, calibration of the system, and aerosol data acquisition. The date the cells were installed in the laboratory allowed for what was considered to be sufficient time for this plan to be implemented. However, unforeseen difficulties arose with the alignment of the optical train and with the operation of the White cell which prevented calibration of the system during the contract period. Only the extinction measurement technique with the White cell was calibrated.

Alignment of the optical train proved to be considerably more difficult than anticipated. The system was susceptible to mechanical instabilities which necessitated complete realignment daily. The most critical aspects of the procedure were the processes of making the He-Ne laser beam collinear with the DF laser beam, and the alignment of the focusing mirror directly ahead of the White cell (M_6 in Figure 2.1). With regard to the former, the f/150 system provided a large uncertainty in the location of the focal plane of the DF beam. This led to a tedious alignment procedure in which the DF and He-Ne beams were checked for colinearity over a 10m range beyond the focal plane.

The most serious optical and mechanical problems, however, arose within the White cell. As delivered to Aerodyne, the cell could not be operated satisfactorily with an internal vacuum. This was due to the adhesive seal holding the mirrors to spring loaded, micrometer mounts, and to the vacuum seal covering these mounts. The mirrors eventually had to be glued to the mounts with a different adhesive. As for the end caps on the cell which provide the vacuum seal, they were so awkward that their installation completely destroyed the optical alignment of the cell.

Optical alignment itself proved to be impossible at long path lengths when the cell was in its original configuration. The 6m mirror spacing was not equipped with an adequate adjustment range to permit focusing of the laser beam on the front mirror when the total optical path length in the cell was ~ 400m or greater. Thus the front mirror mount had to undergo modifications. Even with this adjustment, however, the alignment of the cell was not possible without thermal isolation. The hourly temperature fluctuations in the laboratory produced thermal expansion and contraction along the axis of the White cell which were sufficient throw the mirrors out of alignment. This was finally eliminated by wrapping the cell with a thermostatically controlled heating tape and a 15 cm layer of fiberglas insulation. In this manner, the cell temperature was held to 30 ± 0.5^{o}C, and the thermal distortions were removed.

Only after the above mechanical and thermal modifications were made could the White cell be aligned satisfactorily. The prime concerns then were to prevent the DF laser beam from spilling over the 5 cm diameter back mirrors in the cell, and to center the laser beam in the output aperture drilled in the 15 cm diameter front mirror. Both of these problems were aggravated by the spatial fluctuations in the DF beam itself. Careful consideration of these effects led to sampling the DF beam upstream of the White cell with a 13 mm aperture located at the hot spot in the annular beam. Calibration tests were finally performed with the laser beam tailored in this fashion with a 2 mm spot size at the focal plane at a White cell entrance aperture. At the back mirrors in the cell, the beam diameter was approximately 35 mm. Focusing to smaller diameters at the entrance aperture led to diffraction patterns which more than filled the back mirrors.

The 2 mm diameter pyroelectric detectors proved to be another object of concern. The detectors used were quoted as having a saturation level of 6.4 mJ. However, for the 0.3 μsec laser pulses used in the experiment, saturation was observed at substantially lower values. Indeed, the detector coatings were damaged at lower energies and had to be replaced. In the final configuration, only 10 μJ pulses were incident on the detector surfaces.

After these difficulties were eliminated or at least reduced to what was believed to be tolerable levels, calibration tests were performed on the White cell using a CH_4 - N_2 gas mixture with 500 ppm CH_4. At a 288m path length, the CH_4 absorption coefficient at the DF $P_2(6)$ line was measured to be 0.38 km^{-1} with a scatter of $\pm$ 40%. This is a good agreement with the results of Mills and Long[5] who measured the CH_4 absorption coefficient in a CH_4 - Air mixture. Their data at 500 ppm CH_4 give $k \simeq 0.36$ km^{-1}, while a linear fit to their data taken as a function of CH_4 concentration gives $k \simeq 0.48$ km^{-1}.

The calibration was also performed with a 50 ppm CH_4 concentration in N_2, but the results were less satisfactory. The data gave $k \simeq 0.02 - 0.10$ km^{-1}, while the expected value was $k \simeq 0.04$ km^{-1} for the DF $P_2(6)$ line. The scatter for each set of data runs was 60 - 70%, which combined with the irreproducibility of the data, made the results less than meaningful. After careful realignment of the optics, the calibration tests were repeated. This procedure was followed several times but with no substantial improvement over the results quoted above.

An analysis of these tests indicated that the lack of sensitivity of the system and the scatter in the data were due to two features of the optical train and detection system. First, the scatter in the data was due in large part to the fact that the transmitted and reference beams were focused onto 2 mm diameter pyroelectric detectors. The spot size for both beams was approximately 1.5 mm. Thus, because the shot-to-shot spatial fluctuations of the laser could not be entirely eliminated, the focused spots wandered on and sometimes off the detector elements.

That the scatter was produced by the focusing optics and not the White cell was established when $(V_o - V)/V_o$ (cf. Subsection 2.2.5) was measured without the White cell in the optical train. With the laser beam beam-split twice immediately after the spatial filter and focused into the detectors, we obtained $(V_o - V)/V_o = 0.17 \pm 0.03$, i.e., an 18% error. This was the same as obtained with the White cell.

Second, the signal-to-noise ratios in the data channels were not as large as originally expected. This was due to the necessary tailoring of the laser beam upstream of the White cell and the lower than expected damage threshold of the pyroelectric detectors. In particular, in the $(V_o - V)$ channel in the 1A5 differential amplifier, S/N ~ 20, while in the V_o channel, S/N ~ 200. Based upon these figures and the oscilloscope readout errors, one should expect a 9% error in the $(V_o - V)/V_o$ measurement. The data gave an error that was a factor of 2 greater, which we attribute to the spatial fluctuations of the laser beam.

The above errors were computed for the case where $(V_o - V)$ and V_o must be read separately and the ratio $(V_o - V)/V_o$ determined manually. If as originally planned, $(V_o - V)$ and V_o were monitored and digitized with a transient recorder, then the readout error would be essentially due to the S/N in $(V_o - V)$. In this case, then, the sensitivity and accuracy of the extinction measurement would be limited by the Signal-to-noise ratios and by the laser's spatial fluctuations.

Modifications to the apparatus were devised which would have eliminated these problems, but they could not be implemented because of time constraints of the contract period. Nonetheless, the spatial fluctuations could have been made insignificant if the beams emerging from the White cell were allowed to strike a diffuse scatterer, e.g., a $BaSO_4$ target. If the detector were aligned to observe some fraction of the radiation backscattered from the target, then the spatial fluctuations would not produce fluctuations in the recorded signal, provided the field-of-view of the detector were large enough to include the entire laser spot on target.

We feel confident that these proposed modifications would eliminate the fundamental limitations of the system. If acted upon, they would permit the measurement of aerosol extinction coefficients as small as 0.01 km^{-1}. Combined with the scattering cell apparatus, this would represent a valuable laboratory facility capable of providing data which, to date, have been unavailable to the community.

REFERENCES

1. D.J. Spencer, "Atmospheric Gas Absorption at DF Laser Wavelengths," Proc. of the Meeting on Absorption of Infrared Laser Radiation in the Atmosphere, Mitre Corp., April 4 and 5, 1973.

2. L.D. Gray Young, "Relative Intensity Calculations for Nitrous Oxide," J. Quant. Spectrosc. Rad. Transfer, 12 307 (1972).

3. S.K. Friedlander, "Chemical Element Balances and Identification of Air Pollution Sources," Environ. Sci. Tech. 7, 235 (1973).

4. E.S. Gladney, W.H. Zoller, A.G. Jones, and G.E. Gordon, "Composition and Size Distributions of Atmospheric Particulate Matter in the Boston Area," Environ. Sci. Tech., 8, 551 (1974).

5. F.S. Mills and R.K. Long, "Absorption Coefficient Measurements of CO_2 HDO - N_2, and CH_4 - Air Using a DF Laser," Rome Air Development Center Report RADC-TR-74-295, August, 1974. (A001 097)

MISSION
of
Rome Air Development Center

RADC is the principal AFSC organization charged with planning and executing the USAF exploratory and advanced development programs for information sciences, intelligence, command, control and communications technology, products and services oriented to the needs of the USAF. Primary RADC mission areas are communications, electromagnetic guidance and control, surveillance of ground and aerospace objects, intelligence data collection and handling, information system technology, and electronic reliability, maintainability and compatibility. RADC has mission responsibility as assigned by AFSC for demonstration and acquisition of selected subsystems and systems in the intelligence, mapping, charting, command, control and communications areas.